

Layer-structured hexagonal (BN)C semiconductor alloys with tunable optical and electrical properties

M. R. Uddin, S. Majety, J. Li, J. Y. Lin, and H. X. Jiang^{a)}

Department of Electrical and Computer Engineering, Texas Tech University, Lubbock, Texas 79409, USA

(Received 12 December 2013; accepted 23 February 2014; published online 5 March 2014)

Hexagonal boron nitride carbon, $h(\text{BN})_{1-x}(\text{C}_2)_x$, semiconductor alloys have been grown on sapphire substrates by metal-organic chemical vapor deposition. Bandgap tuning through compositional variation has been demonstrated via optical absorption measurements. Furthermore, an enhancement of approximately 10 orders of magnitude in the electrical conductivity has been attained by increasing the carbon concentration (x) from 0 to 0.21. Experimental results revealed evidences that the critical carbon concentration x_c to form the homogenous $h(\text{BN})_{1-x}(\text{C}_2)_x$ alloys, or the carbon solubility in hBN is about 3.2% at a growth temperature of 1300 °C before carbon clusters form. Based on the predicted phase diagram of cubic $(\text{BN})_{1-x}(\text{C}_2)_x$ and the excellent matches in the structural and thermal properties of hBN and graphite, it is expected that homogenous $h(\text{BN})_{1-x}(\text{C}_2)_x$ alloys with higher x can be achieved and the alloy miscibility gap can be reduced or completely removed by increasing the growth temperature. This is a huge advantage over the InGaN alloy system in which InN decomposes at high temperatures and high growth temperature cannot be utilized to close the miscibility gap. The results indicate that the $h(\text{BN})_{1-x}(\text{C}_2)_x$ alloy system has the potential to tackle the challenging issues facing the emerging two-dimension materials beyond graphene, which include realizing the bandgap engineering, conductivity control, and large wafers of homogeneous films. © 2014 AIP Publishing LLC.

[<http://dx.doi.org/10.1063/1.4867641>]

I. INTRODUCTION

Hexagonal boron nitride (hBN) is a layer-structured semiconductor material with a bandgap energy that is comparable to that of AlN (~6 eV) with excellent thermal, mechanical, and optical properties.^{1–8} Following the isolation of graphene,⁹ intensive research activities are currently being undertaken worldwide in the areas beyond graphene–two dimensional (2D) materials with non-zero energy band gaps. Due to the identical crystalline structure and nearly perfect lattice constant matches to graphene, hBN has been recognized as an excellent template or dielectric layer for graphene electronic/photonic devices.^{10–12} The technique of manually separating individual layers from layer-structured crystals and stacking them has been very effective in demonstrating the rich physics of 2D materials. This method obviously has disadvantages of producing materials with small size (~100 μm) due to the limited size of hBN bulk crystals and is not scalable. Furthermore, graphene/hBN heterostructures offer limited prospect in providing the ability for bandgap engineering.

Both hBN and graphite have layer structures with similar lattice parameters and crystalline structures. The in-plane lattice constant difference is only about 1.5% between graphite and hBN. Although BN has many forms, its most stable crystalline structure for materials prepared under ambient pressure at any temperature is hexagonal.^{1–3,13,14} The similarity between hBN and graphite provides potential to synthesize layer-structured $h(\text{BN})_{1-x}(\text{C}_2)_x$ alloys. We are using

the expression of $(\text{BN})_{1-x}(\text{C}_2)_x$ for these alloys to take into consideration the fact that C atoms tend to incorporate as C-C (C_2) pairs.¹⁵ The $(\text{BN})_{1-x}(\text{C}_2)_x$ alloy system holds the unique advantages of identical crystalline structure (hexagonal) and excellent matches in lattice constants, thermal expansion coefficients, and melting temperatures throughout the entire alloy range.¹⁴ Nevertheless, if homogeneous alloys can be synthesized, the $h(\text{BN})_{1-x}(\text{C}_2)_x$ system possesses an extremely large energy gap variation from around 6 eV (hBN) to 0 (graphite), covering a spectral range from deep ultraviolet to far infrared. This spectral range is even larger than that of the InAlGaN alloy system could reach (InAlGaN provides tunable bandgaps from around 0.64 eV (InN) to 3.4 eV (GaN) to 6.1 eV (AlN)). From an electrical properties perspective, this alloy system ranges from highly insulating semiconductor (undoped hBN) to semi-metal (graphite), and therefore, a large range of conductivity control can be obtained. If homogeneous alloys can be synthesized, the $h(\text{BN})_{1-x}(\text{C}_2)_x$ material system would address the major challenges facing the emerging 2D materials systems and open up new realms for novel physical properties and devices exploration.

A recent theoretical calculation suggests that it is possible to open a small bandgap in graphene by doping graphene with BN domains.¹⁶ Atomic layers consisting of hybridized, randomly distributed domains of hBN and C phases with compositions ranging from pure BN to pure graphene were obtained by a chemical vapor deposition growth technique.¹⁷ However, as with any new semiconductor materials in the development stages, the ability for synthesizing large wafers of homogeneous alloys (instead of domains) is a prerequisite

^{a)}Email: hx.jiang@ttu.edu

for the realization of technologically significant device applications. Like many semiconductor alloy systems, one of the critical questions is the issue of phase separation and the range of homogeneous alloys that can be formed. Phase separation occurs in semiconductor alloys that are composed of constituents with significant differences in lattice constants or bond energies. Alloying in (BN)C system is challenging due to the strong bonds between B-N and C-C, which have respective bond energies of 4.0 eV (B-N) and 3.71 eV (C-C) compared with values of 2.83 eV for the C-N bond and 2.59 eV for the C-B bond.^{15,18} There were, however, theoretical and experimental evidences for obtaining homogeneous $(\text{BN})_x(\text{C}_2)_{1-x}$ alloys with $x = 0.5$ (BNC_2) and that BNC_2 is a direct bandgap semiconductor with an estimated bandgap energy $E_g = 2.0$ eV.^{18,19}

In this work, we report on the synthesis of $h(\text{BN})_{1-x}(\text{C}_2)_x$ epilayers with tunable energy bandgap and electrical conductivity by metal organic chemical vapor deposition (MOCVD). MOCVD is an established technique for producing high quality crystalline materials due to its ability to precisely control the growth processes and has been widely adopted by the commercial world for the growth of other compound semiconductor materials, particularly III-nitrides, in large wafer scales. Our experimental results provide evidence that homogeneous $h(\text{BN})_{1-x}(\text{C}_2)_x$ alloys with $x \leq 3.2\%$ have been synthesized by MOCVD. Bandgap tuning through compositional variation has been demonstrated. We also discuss possible routes to increase the solubility of C in $h(\text{BN})_{1-x}(\text{C}_2)_x$ alloys.

II. EXPERIMENT

Epitaxial layers of $h(\text{BN})_{1-x}(\text{C}_2)_x$ alloys of about 60 nm in thickness were synthesized on sapphire (0001) substrates using triethylboron (TEB), ammonia (NH_3), and propane (C_3H_8) as B, N, and C sources, respectively. Samples were grown using hydrogen as a carrier gas at 1300 °C (temperature limit of our current MOCVD system). Seven samples, denoted as A, B, C, D, E, F, and G were grown at C_3H_8 flow rates of 0 (hBN), 0.5, 1, 2, 3, 4, and 5 standard cubic centimeters (scm) per minute, respectively. Crystalline structure was determined by x-ray diffraction (XRD) measurements. UV-visible (UV-vis) optical absorption spectroscopy was employed to determine the optical absorption edges. Both van der Pauw and I-V characteristics measurements were performed to compare the relative electrical resistivities of $h(\text{BN})_{1-x}(\text{C}_2)_x$ epilayers with varying C concentrations. Composition x was determined using x-ray photoelectron spectroscopy (XPS), which is a quantitative spectroscopic technique to determine the elemental composition, chemical bonding, and chemical state of the elements in a material system. Carbon concentrations (C) of samples A, B, C, D, E, F, and G, determined by XPS, were 0%, 1.7%, 3.2%, 6%, 10%, 14%, and 21%, respectively. The XRD θ - 2θ scan patterns of $h(\text{BN})_{1-x}(\text{C}_2)_x$ samples have a similar spectral shape. Figure 1(a) shows XRD θ - 2θ scan of a representative hBN epilayer deposited on sapphire substrate, revealed a c -lattice constant of ~ 6.67 Å, which closely matches with the bulk

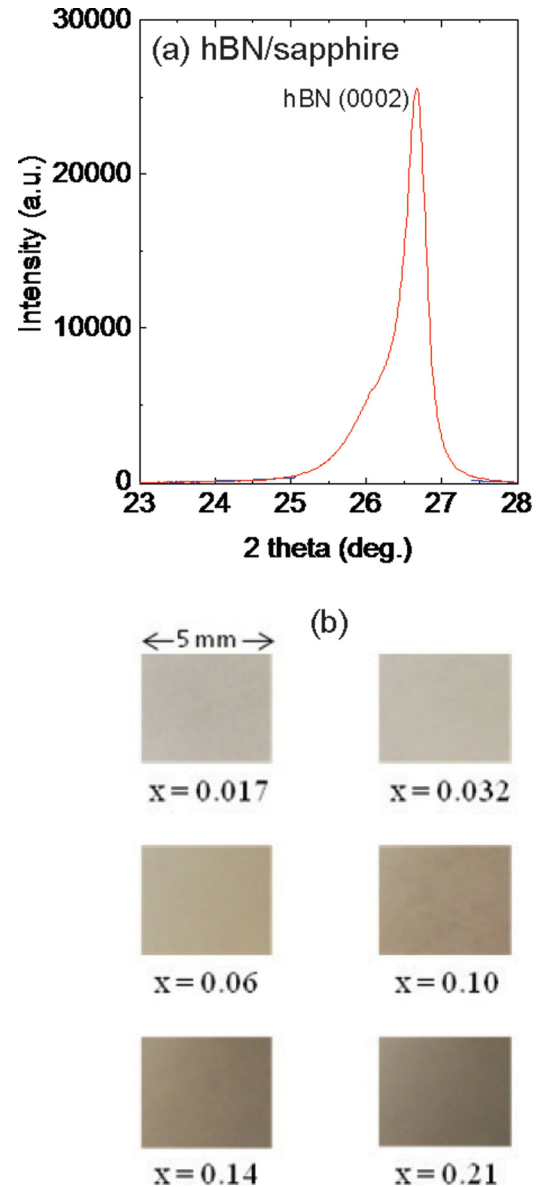


FIG. 1. (a) XRD θ - 2θ scan pattern of an hBN epilayer deposited on sapphire substrate. (b) Optical micrographs (5 mm \times 5 mm) of $h(\text{BN})_{1-x}(\text{C}_2)_x$ epilayers with different C concentrations deposited on sapphire substrates.

c -lattice constant of hBN ($c = 6.66$ Å),^{13,14} affirming that the MOCVD grown films have a hexagonal lattice structure.

III. RESULTS AND DISCUSSION

Figure 1(b) shows the optical micrographs of 5 mm \times 5 mm area of $h(\text{BN})_{1-x}(\text{C}_2)_x$ epilayers with different carbon concentrations. A previous calculation¹⁸ hinted that due to the strong C-C bonds, C atoms tend to form clusters in (BN)C alloys when C concentration is above a certain critical value, x_c . This effect can be directly observed from the optical micrographs of our $h(\text{BN})_{1-x}(\text{C}_2)_x$ epilayers. Based on the bandgap value of hBN (~ 6 eV) and the small values of x ($x = 0$ to 0.21), these $h(\text{BN})_{1-x}(\text{C}_2)_x$ epilayers should be transparent in the visible spectral range. However, only samples with $x = 0, 0.017$, and 0.032 are transparent. Samples with $x = 0.06, 0.10, 0.14$, and 0.21 appear dark and the darkness increases with an increase of x . We believe that this is

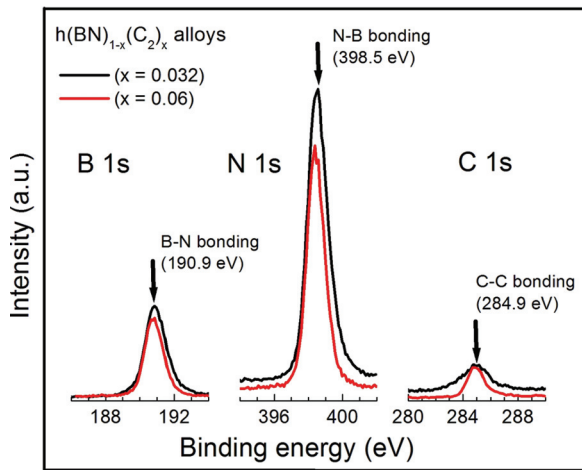


FIG. 2. XPS spectra of (a) B 1s, (b) N 1s, and (c) C 1s core levels for the $h(\text{BN})_{1-x}(\text{C}_2)_x$ epilayers with $x = 0.032$ and 0.06 .

due to the formation of C clusters in these alloys, which is further corroborated by the XPS and optical absorption spectra to be discussed below. The results shown in Fig. 1(b) seem to suggest that the critical C concentration, x_c , for homogeneous alloy formation, or the solid solubility limit of C in $h\text{BN}$ is around 0.032 for the growth temperature of 1300°C .

Figure 2 shows the XPS spectra of B 1s, N 1s, and C 1s core levels for two representative $h(\text{BN})_{1-x}(\text{C}_2)_x$ alloy samples with $x = x_c$ (≈ 0.032) and $x = 0.06$. Atomic composition of B, N, and C was determined from the tight scans. We would like to point out that the sample surface is easily contaminated by impurities from atmosphere. To eliminate the surface contamination before XPS measurements, we

followed the procedure of low energy Ar^+ ion dusting and soft etching, which completely removed any surface contaminations, such as carbon and oxygen. After removing the surface contaminations, atomic compositions of B, N, and C become constant inside the film, which was verified by the depth profile measurements carried out for selective samples. A comprehensive XPS analysis of all $h\text{BNC}$ samples will be reported elsewhere.

Figures 3(a)–3(c) show the XPS spectra of B 1s, N 1s, and C 1s, respectively, obtained for a representative $h(\text{BN})_{1-x}(\text{C}_2)_x$ sample with $x = 0.032$. The B 1s spectral peak is at 190.9 eV in agreement with a previous report,¹¹ which corresponds to three N atoms bonding with one B atom in the center (area 1), as schematically illustrated in the inset of Fig. 3(a). The full width at half maximum (FWHM) of the peak is ~ 1.5 eV, which is larger than that of $h\text{BN}$ (~ 0.9 eV). A small peak (area 2) at 189.3 eV is due to the B-C bonding, because of the lower electronegativity of C than N.²⁰ The N 1s spectral peak at 398.5 eV shown as area 1 in Fig. 3(b), which is close to the peak position reported for BNC_2 (398.7 eV),²¹ corresponds to three B atoms bonded with one N atom in the center, as schematically shown in the inset of Fig. 3(b). Besides the N-B bond, the peak at 399.4 eV (area 2, Fig. 3(b)) is due to the contribution from N-C bonds, as the electronegativity of C is higher than that of B.²¹ Figure 3(c) shows the spectrum for C 1s. Area 1 of Fig. 3(c) shows the main peak at 284.9 eV, which is similar to that of graphite. However, the FWHM of this peak is 1.55 eV, significantly larger than that of pure graphite (0.35 eV).²¹ This confirms that there is a significant contribution from C-B and C-N bonds in this alloy system. There are two additional peaks in the left and right sides of the main peak, indicated as area 2 and area 3, respectively. The lower energy peak at

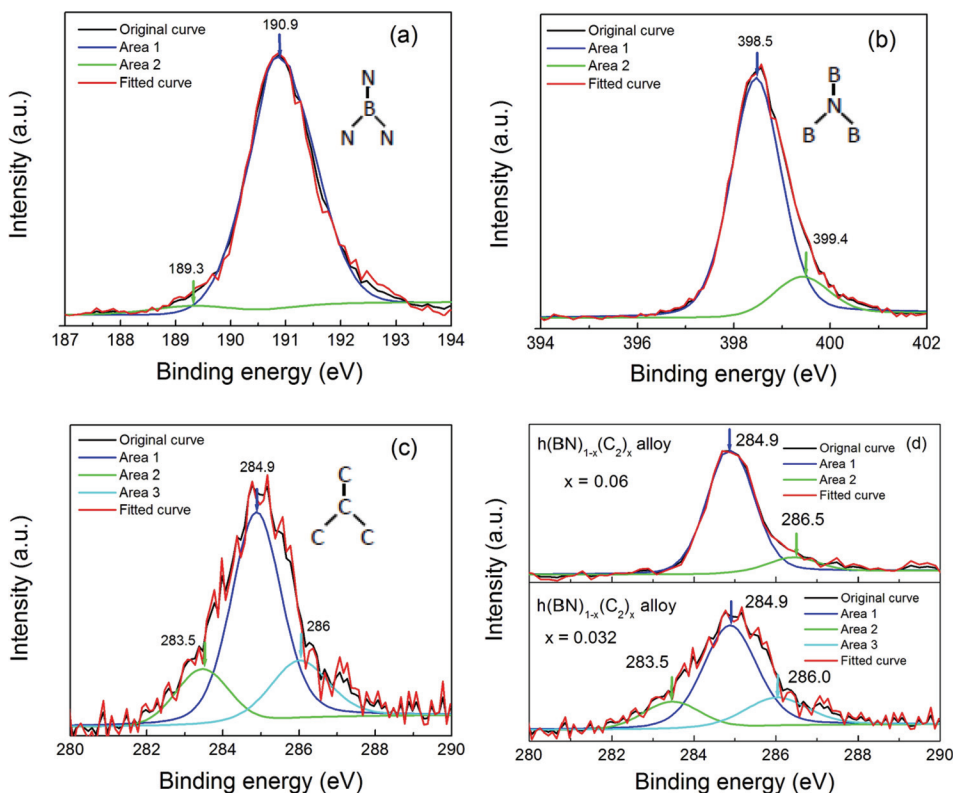


FIG. 3. XPS spectra of (a) B 1s, (b) N 1s, and (c) C 1s core levels for the $h(\text{BN})_{1-x}(\text{C}_2)_x$ epilayer with $x = x_c$ (≈ 0.032). (d) Comparison of the C-C bonding peak with respect to the C-N and C-B bonding peaks for the samples with $x = x_c$ (≈ 0.032) and $x = 0.06$.

283.5 eV (area 2) is due to C bonding with B, as the electronegativity of B is lower than that of C. The higher energy peak at 286 eV (area 3) is due to C bonding with N, because the electronegativity of N is higher than that of C. This is consistent with earlier XPS data for B_4C compounds.²² The chemical shifts, peak broadening, and bonding analysis described above indicate that boron, carbon, and nitrogen atoms bond with one another, and mix atomically.

Figure 3(d) compares the C 1s spectra of $h(BN)_{1-x}(C_2)_x$ alloys with $x = x_c$ (≈ 0.032) and $x = 0.06$. Peak position of area 1 for both samples at 284.9 eV is due to C-C bonds. The peak at 286.0 eV and 283.5 eV for the sample with $x = x_c$ (≈ 0.032) is due to C bonding with N and C bonding with B, respectively. The peak at 286.5 eV for the sample with $x = 0.06$ is due to C bonding with N. If we compare the main C-C bonding peak with respect to the C-N bonding peak between the two samples, it is obvious that the C-C bonding peak is more dominant in the sample with $x = 0.06$. A strong C-C bonding peak is the signature of the formation of C clusters. Also, C-B bonds are negligible in the sample with $x = 0.06$ since the peak at 283.5 eV corresponding to C-B bonds is absent in this sample. This is due to the fact that the C-B bond energy (2.59 eV) is less than that of C-N (2.83 eV).¹⁵ The formation of C clusters in samples with $x > x_c$ is also supported by the optical absorption results shown in Figs. 4 and 5 below.

Experimental data on fundamental optical properties of $h(BN)_{1-x}(C_2)_x$ alloys are scarce with an exception for one particular C concentration $x = 0.5$ (BNC_2), which has an estimated bandgap energy $E_g = 2.0$ eV based on the spectroscopic measurements of scanning tunneling microscopy.¹⁹ In this work, UV-visible optical absorption spectroscopy was employed to measure the bandgap variation with C incorporation. We have observed that the optical absorption edge of $h(BN)_{1-x}(C_2)_x$ epilayers decreases with an increase of the C concentration, as expected. The absorption coefficients (α) were obtained from the absorption spectrum. The energy bandgap E_g values were estimated from the Tauc plot of the absorption coefficients.²³ In Fig. 4, we plot α^2 as a function of the excitation photon energy for $h(BN)_{1-x}(C_2)_x$ epilayers with $x = 0.0, 0.017, 0.032, 0.06, 0.10, 0.14,$ and 0.21 . E_g

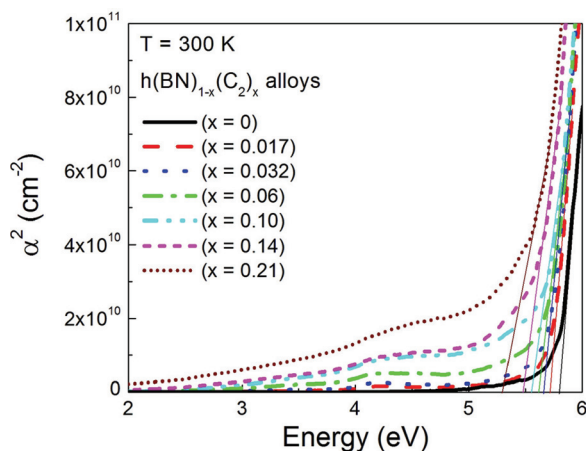


FIG. 4. Tauc plots of absorption coefficients of $h(BN)_{1-x}(C_2)_x$ epilayers with different C concentrations.

values are obtained from the intersections between the straight lines and the horizontal axis. E_g values of 5.80 eV, 5.70 eV, 5.65 eV, 5.60 eV, 5.55 eV, 5.47 eV, and 5.30 eV were obtained for samples A, B, C, D, E, F, and G, respectively, which are listed in Table I. The measured optical absorption edge of 5.8 eV for hBN agrees with a previous measurement²⁴ and coincides well with the onset energy

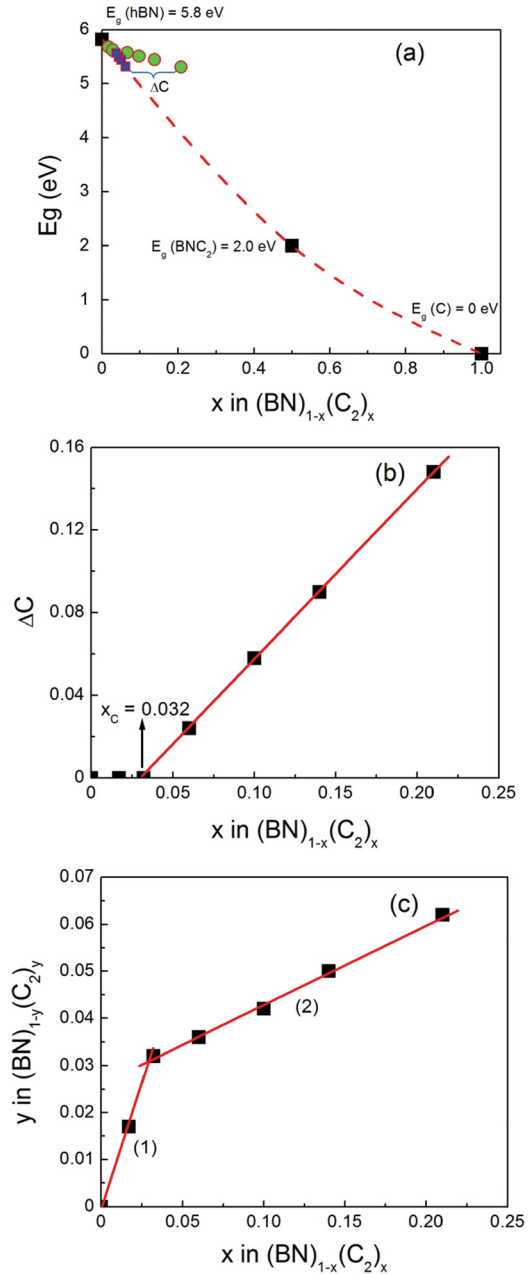


FIG. 5. (a) Energy bandgap E_g versus C concentration in $h(BN)_{1-x}(C_2)_x$ alloys. Green filled circles are the measured data of E_g obtained from the optical absorption spectra and the total C concentrations from XPS. Blue filled squares are the data points extrapolated from Eq. (1) representing the C concentrations in the homogeneous $h(BN)_{1-x}(C_2)_x$ alloys (y), which is lower than the total C concentration in the samples (x). ΔC indicates the amount of excess C concentration in $h(BN)_{1-x}(C_2)_x$ alloys with $x > x_c$ (≈ 0.032), which ends up in the separated C phase. In the plot, we take E_g (graphite) = 0 eV and E_g (BNC_2) = 2.0 eV.¹⁹ (b) The plot of ΔC versus x in $h(BN)_{1-x}(C_2)_x$ alloys. (c) The plot of the C concentration in the homogeneous $h(BN)_{1-y}(C_2)_y$ alloy phase (y) versus the total C concentration in the $h(BN)_{1-x}(C_2)_x$ samples (x).

TABLE I. List of samples with different C_3H_8 flow rates. Carbon concentrations (x) and energy bandgaps of the $h(BN)_{1-x}(C_2)_x$ epilayers are measured by XPS and optical absorption, respectively. ΔC indicates the excess C concentration in $h(BN)_{1-x}(C_2)_x$ samples with $x > x_c$ (≈ 0.032), which ends up in a separated carbon (or graphite) phase.

Sample	C_3H_8 flow (sccm)	x in $h(BN)_{1-x}(C_2)_x$ (measured by XPS)	ΔC	E_g (eV)
A	0	0	0	5.8
B	0.5	0.017	0	5.7
C	1.0	0.032	0	5.65
D	2.0	0.06	0.024	5.6
E	3.0	0.10	0.058	5.55
F	4.0	0.14	0.09	5.47
G	5.0	0.21	0.148	5.3

position of the excitonic emission line.^{8,25} The results suggest that the optical absorption edge is strongly affected by the excitonic effects and the actual bandgap of hBN is expected to be greater than the measured value by an amount of the exciton binding energy, which is around 0.7 eV.^{25–28}

Figure 5(a) plots the measured E_g vs. x for $h(BN)_{1-x}(C_2)_x$ epilayers that include the bandgap energies of hBN ($x=0$), graphite, and $h(BNC_2)$ from Ref. 19. The dashed curve represents a fitting using the general equation for describing the bandgaps of semiconductor ternary alloys,

$$Eg[h(BN)_{1-x}(C_2)_x] = (1-x)Eg(hBN) + xEg(C) - b(1-x)x, \quad (1)$$

where x is the mole fraction of C in the $h(BN)_{1-x}(C_2)_x$ alloys and b is the bowing parameter. $E_g(C)=0$ is the energy bandgap of graphite. The fitted bowing parameter is $b=3.6$ eV. The green filled circles are the measured C concentrations obtained from XPS and the corresponding E_g values obtained from the optical absorption spectra. The results show that the data for samples with $x=0.017$ and 0.032 fit well with Eq. (1), suggesting the formation of homogeneous alloys.

Samples with $x=0.06, 0.10, 0.14,$ and 0.21 deviate significantly from Eq. (1). This can be explained by the fact that phase separation occurs in samples with $x > x_c$ (≈ 0.032). In the phase separated materials, the XPS measures the total C concentrations, while the C concentration deduced from the bandgap variation of Eq. (1) represents the C concentration in homogeneous alloy phase. Therefore, the deviation from Eq. (1) is a measure of the excess C concentration in the phase separated C clusters (graphite phase). In other words, $h(BN)_{1-x}(C_2)_x$ alloys with $x > x_c$ (≈ 0.032) have separated C phases and the actual C concentrations in the homogeneous alloys (y) are less than the total C concentration determined by XPS (x). In addition, the C concentration in homogeneous alloys (y) can be determined from E_g measured by the optical absorption spectroscopy coupled with the use of Eq. (1). From this procedure, we plot the data for the C concentrations in the homogeneous alloy phase (y) as blue filled squares in Fig. 5(a). The C concentration difference between x and y is denoted as $\Delta C = x - y$ (indicated in the figure). So, ΔC measures the excess carbon concentrations that are in the

separated C phases (or graphite phase) in samples D, E, F, and G. However, at $x > x_c$, phases of hBN , graphite, and $h(BN)_{1-y}(C_2)_y$ alloys with $y < x$ coexist.

Figure 5(b) shows ΔC versus the total C concentration x in $h(BN)_{1-x}(C_2)_x$ alloys. For samples B and C with $x=0.017$ and 0.032 , $\Delta C=0$, which means that these materials with low x form homogeneous alloys (or are completely miscible). The solid line in Fig. 5(b) is a linear fit of data with the equation

$$\Delta C = b(x - x_c) \text{ for } x > x_c, \quad (2)$$

where ΔC is the C concentration in the graphite phase and x is the total C concentration measured by XPS. The fitted values of b and x_c are 0.83 and 0.032, respectively. The physical meaning of Fig. 5(b) and Eq. (2) is that for samples grown at $1300^\circ C$ with C concentrations larger than x_c (≈ 0.032), about 83% of C will be in the separated C phase, while the remaining 17% will be in the homogeneous alloy phase. It is expected that x_c will be increased and the red line will be shifted to the right with an increase in the growth temperature. However, currently we are unable to estimate the percentage of C in the graphite phase at higher growth temperatures.

To present these results in a different way, Fig. 5(c) shows the C concentration in the homogeneous $h(BN)_{1-y}(C_2)_y$ alloy phase (y) deduced from the energy bandgap obtained from optical absorption spectra versus the total C concentration in $h(BN)_{1-x}(C_2)_x$ samples measured by XPS (x). Two distinctive regions of alloying are obtained from the linear fits of the data using equations

$$\begin{aligned} y &= a_1 x & \text{for } 0 \leq x \leq x_c, \\ y &= b + a_2 x & \text{for } x > x_c. \end{aligned} \quad (3)$$

The fitted value of a_1 is 1 meaning that at $x \leq x_c$ (≈ 0.032), the C concentration in the homogeneous $h(BN)_{1-x}(C_2)_x$ alloy phase equals to the total C concentration measured by XPS, or $y=x$. The fitted values of a_2 and b for line (2) are 0.17 and 0.026, respectively. This implies that the C concentration in the homogeneous $h(BN)_{1-y}(C_2)_y$ alloy phase (y) also increases with an increase of the total C concentration x for samples with $x > x_c$ (≈ 0.032). Our results thus suggest that a small fraction ($\sim 17\%$) of C still incorporates into the homogeneous $h(BN)_{1-x}(C_2)_x$ alloy phase beyond the critical concentration and that homogeneous $h(BN)_{1-x}(C_2)_x$ alloys with x as high as 6.3% can be achieved even at the growth temperatures of $1300^\circ C$. However, phase separated C clusters co-exist in these samples.

Another unique feature of the $h(BN)_{1-x}(C_2)_x$ alloy system is that it offers the conductivity variation from highly insulating semiconductor (undoped hBN) to semi-metal (graphite). Figure 6 shows the 300 K electrical resistivity for samples with different C concentrations. In obtaining Fig. 6, we adopted ohmic contacts preparation processes previously developed for hBN .⁷ The ohmic contacts consist of Ni/Au (30 nm/20 nm) bilayers, which were deposited using e-beam evaporation followed by rapid thermal annealing at $800^\circ C$ for 10 min. The schematic of a fabricated $h(BN)C$ sample

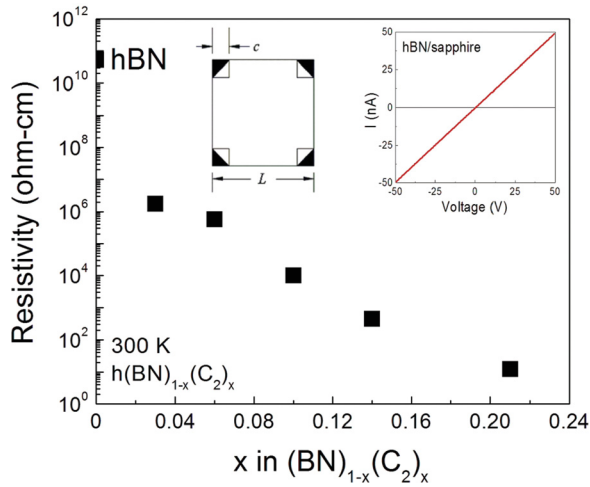


FIG. 6. Room temperature resistivity of $h(\text{BN})_{1-x}(\text{C}_2)_x$ alloys as a function of the total C concentration measured by XPS (x). The two insets show the schematic of the sample geometry for electrical transport measurements and the demonstrated ohmic behavior of the I-V characteristics for an undoped hBN epilayer. The four ohmic contacts on the corners of the sample consist of Ni/Au (30 nm/20 nm) bilayers and were deposited using e-beam evaporation followed by rapid thermal annealing at 800 °C for 10 min. The contact size (c) to the sample length scale (L) is about 1/5.

and ohmic contact (Ni/Au bilayers) geometry employed for the electrical measurements is shown in the insets of Fig. 6. The typical I-V characteristics of undoped hBN epilayers, which have the highest resistivity among $h(\text{BN})_{1-x}(\text{C}_2)_x$ epilayers are shown in the inset of Fig. 6 and exhibit an excellent ohmic behavior. Both van der Pauw and I-V characteristics measurements were performed to compare the relative electrical resistivities of $h(\text{BN})_{1-x}(\text{C}_2)_x$ epilayers with varying C concentrations. We observe that the electrical resistivity decreases approximately by 10 orders of magnitude when x increases from 0 to 0.21. Since graphite is a semimetal and undoped hBN is highly insulating, it is expected that when these two systems combine to form $h(\text{BN})_{1-x}(\text{C}_2)_x$ alloys, a large range of electrical conductivity control can be achieved and the electrical conductivity increases with an increase of C concentration. Moreover, in the case of $x > x_c$, the formation of C clusters further increases the electrical conductivity.

Phase separation has been a long outstanding issue for InGaN alloys, and still remains to be solved. Although not much information is available on the phase separation issue in $h(\text{BN})_{1-x}(\text{C}_2)_x$ alloys, we can briefly summarize the differences between InGaN and $h(\text{BN})_{1-x}(\text{C}_2)_x$ alloys in terms of phase separation. Phase separation in InGaN alloys is mainly caused by the difference in the in-plane a -lattice constants between InN ($a = 0.3544$ nm) and GaN ($a = 0.3189$ nm),^{29,30} whereas the difference in bond energies between B-N (4.0 eV), C-C (3.71 eV), C-N (2.83 eV), and C-B (2.59 eV) is the main cause of the phase separation in $h(\text{BN})_{1-x}(\text{C}_2)_x$ alloys.¹⁸ In addition to the lattice constants mismatch between InN and GaN, the growth temperature mismatch between InN and GaN makes the phase separation issue in InGaN even more difficult to overcome.³¹ Theoretically, increasing the growth temperature will reduce the miscibility gap,²⁹ but InN decomposes at high temperatures ($T > 700$ °C). While the

crystalline quality of InGaN alloys can be improved by employing low growth rate in the low In-content regime,³¹ growth conditions farther away from the thermodynamic equilibrium (such as high growth rates) are helpful to promote the formation of single phase InGaN alloys in the theoretically predicted miscibility gap region (middle range of the alloy composition).³²

It appears that phase separation is also a significant challenge to the synthesis of homogeneous $h(\text{BN})_{1-x}(\text{C}_2)_x$ alloys. Recent theoretical calculation performed on monolayer cubic $c(\text{BN})_{1-x}(\text{C}_2)_x$ suggests a low solubility of C at the growth temperature of 1300 °C.³³ The calculated phase diagram of the monolayer $c(\text{BN})_{1-x}(\text{C}_2)_x$ materials in the temperature range of 1500-3500 K shows that the miscibility gap decreases with an increase in the growth temperature.³³ The same trend is expected for $h(\text{BN})_{1-x}(\text{C}_2)_x$ alloys. Due to the excellent matches in lattice constants, thermal expansion coefficients, and melting temperatures throughout the entire alloys, it is expected that the alloy miscibility gap in $h(\text{BN})_{1-x}(\text{C}_2)_x$ alloys can be reduced or completely removed by increasing the growth temperature. This is a huge advantage over InGaN in which InN decomposes at high temperatures and high growth temperature cannot be utilized to close the miscibility gap. It is also expected that the crystalline quality of $h(\text{BN})\text{C}$ alloys will be improved at the higher growth temperatures.

IV. CONCLUSIONS

In summary, we have synthesized via MOCVD $h(\text{BN})_{1-x}(\text{C}_2)_x$ epilayers with different C concentrations. Our experimental results revealed evidences that the critical C concentration x_c to form homogenous $h(\text{BN})_{1-x}(\text{C}_2)_x$ alloys, or the C solubility in hBN is about 3.2% at a growth temperature of 1300 °C before C clusters form. Furthermore, we have achieved variations in the energy bandgap and electrical conductivity in $h(\text{BN})_{1-x}(\text{C}_2)_x$ epilayers through the variation in C concentration. We believe that raising the growth temperature above 1300 °C will allow us to synthesize $h(\text{BN})_{1-x}(\text{C}_2)_x$ alloys with improved crystalline quality as well as with higher C concentrations without C clusters. Currently, our understanding of $h(\text{BN})_{1-x}(\text{C}_2)_x$ alloy is still in a very early stage and many issues merit further studies. These include detailed studies on the structural properties of the films by various methods to provide improved understandings on the correlation between the growth conditions and structural and optoelectronic properties; the alloy dependence of the optical and electrical properties and band structures near the fundamental band edge; the evolution of the electrical conductivity from semi-metal to insulating or to semiconductor within the same crystal structure; the feasibility of conductivity control via *in situ* doping by MOCVD growth; and potential applications of this unique layer-structured $(\text{BN})_x(\text{C}_2)_{1-x}$ alloy system with bandgap variation from far infrared to deep UV.

ACKNOWLEDGMENTS

This work was supported by NSF (DMR-1206652). H. X. Jiang and J. Y. Lin are grateful to the AT&T Foundation

for the support of Ed Whitacre and Linda Whitacre endowed chairs. The authors are grateful to Dr. Kate Ziemer for valuable discussions on XPS results.

- ¹N. G. Chopra, R. J. Luyken, K. Cherrey, V. H. Crespi, M. L. Cohen, S. G. Louie, and A. Zettl, "Boron-Nitride Nanotubes," *Science* **269**, 966 (1995).
- ²A. Rubio, J. L. Corkill, and M. L. Cohen, *Phys. Rev. B* **49**, 5081 (1994).
- ³J. Wu, W.-Q. Han, W. Walukiewicz, J. W. Ager III, W. Shan, E. E. Haller, and A. Zettl, *Nano Lett.* **4**, 647 (2004).
- ⁴K. Watanabe, T. Taniguchi, and H. Kanda, *Nature Mater.* **3**, 404 (2004).
- ⁵R. Dahal, J. Li, S. Majety, B. N. Pantha, X. K. Cao, J. Y. Lin, and H. X. Jiang, *Appl. Phys. Lett.* **98**, 211110 (2011).
- ⁶J. Li, S. Majety, R. Dahal, W. P. Zhao, J. Y. Lin, and H. X. Jiang, *Appl. Phys. Lett.* **101**, 171112 (2012).
- ⁷S. Majety, J. Li, X. K. Cao, R. Dahal, B. N. Pantha, J. Y. Lin, and H. X. Jiang, *Appl. Phys. Lett.* **100**, 061121 (2012).
- ⁸K. Watanabe and T. Tanniguchi, *Phys. Rev. B* **79**, 193104 (2009).
- ⁹A. K. Geim and K. S. Novoselov, *Nature Mater.* **6**, 183 (2007).
- ¹⁰N. Alem, R. Erni, C. Kisielowski, M. D. Rossell, W. Gannett, and A. Zettl, *Phys. Rev. B* **80**, 155425 (2009).
- ¹¹R. V. Gorbachev, I. Riaz, R. R. Nair, R. Jalil, L. Britnell, B. D. Belle, E. W. Hill, K. S. Novoselov, K. Watanabe, T. Taniguchi, A. K. Geim, and P. Blake, *Small* **7**, 465 (2011).
- ¹²C. R. Dean, A. F. Young, I. Meric, C. Lee, L. Wang, S. Sorgenfrei, K. Watanabe, T. Taniguchi, P. Kim, K. L. Shepard, and J. Hone, *Nat. Nanotechnol.* **5**, 722 (2010).
- ¹³R. S. Pease, "An X-ray study of boron nitride," *Acta Crystallogr.* **5**, 356 (1952).
- ¹⁴S. L. Rumyantsev, M. E. Levinshtein, A. D. Jackson, S. N. Mohammad, G. L. Harris, M. G. Spencer, and M. S. Shur, in *Properties of Advanced Semiconductor Materials GaN, AlN, InN, BN, SiC, SiGe*, edited by M. E. Levinshtein, S. L. Rumyantsev, and M. S. Shur (John Wiley & Sons, Inc., New York, 2001), pp. 67–92.
- ¹⁵S. Bahandary and B. Sanyal, *Graphene-Boron Nitride Composite: A Material with Advanced Functionalities* (InTech, 2012).
- ¹⁶X. Fan, Z. Shen, A. Q. Liu, and J. Kuo, *Nanoscale* **4**, 2157 (2012).
- ¹⁷L. Ci, L. Song, C. Jin, D. Jariwala, D. Wu, Y. Li, A. Srivastava, Z. Wang, K. Storr, L. Balicas, F. Liu, and P. M. Ajayan, *Nature Mater.* **9**, 430 (2010).
- ¹⁸H. Nozaki and S. Itoh, *J. Phys. Chem. Solids* **57**, 41 (1996).
- ¹⁹M. O. Watanabe, S. Itoh, T. Sasaki, and K. Mizushima, *Phys. Rev. Lett.* **77**, 187 (1996).
- ²⁰M. Kawaguchi, T. Kawashima, and T. Nakajima, *Chem. Mater.* **8**, 1197 (1996).
- ²¹M. O. Watanabe, S. Itoh, K. Mizushima, and T. Sasaki, *Appl. Phys. Lett.* **68**, 2962 (1996).
- ²²H. Kunzli, P. Gantenbein, R. Steiner, and P. Oelhafen, *J. Fresenius, J. Anal. Chem.* **346**, 41 (1993).
- ²³D. M. Hoffman, G. L. Doll, and P. C. Eklund, *Phys. Rev. B* **30**, 6051 (1984).
- ²⁴A. Zunger, A. Katzir, and A. Halperin, *Phys. Rev. B* **13**, 5560 (2013).
- ²⁵X. K. Cao, B. Clubine, J. H. Edgar, J. Y. Lin, and H. X. Jiang, *Appl. Phys. Lett.* **103**, 191106 (2013).
- ²⁶B. Arnaud, S. Lebègue, P. Rabiller, and M. Alouani, *Phys. Rev. Lett.* **96**, 026402 (2006).
- ²⁷B. Arnaud, S. Lebègue, P. Rabiller, and M. Alouani, *Phys. Rev. Lett.* **100**, 189702 (2008).
- ²⁸L. Wirtz, A. Marini, and A. Rubio, *Phys. Rev. Lett.* **96**, 126104 (2006).
- ²⁹I.-H. Ho and G. B. Stringfellow, *Appl. Phys. Lett.* **69**, 2701 (1996).
- ³⁰R. Singh, D. Doppalapudi, T. D. Moustakas, and L. T. Romano, *Appl. Phys. Lett.* **70**, 1089 (1997).
- ³¹S. Nakamura and G. Fasol, *The Blue Laser Diode* (Springer, Berlin, 1997), pp. 201–260.
- ³²B. N. Pantha, J. Li, J. Y. Lin, and H. X. Jiang, *Appl. Phys. Lett.* **96**, 232105 (2010).
- ³³K. Yuge, *Phys. Rev. B* **79**, 144109 (2009).